

Research papers

Mapping inundation dynamics in a heterogeneous floodplain: Insights from integrating observations and modeling approach

Zhiqiang Tan^a, Yunliang Li^a, Xiuli Xu^b, Jing Yao^a, Qi Zhang^{a,*}

^a Key Laboratory of Watershed Geographic Sciences, Nanjing Institute of Geography and Limnology, Chinese Academy of Sciences, 73 East Beijing Road, Nanjing 210008, PR China

^b College of Water Resources Science and Engineering, Taiyuan University of Technology, Taiyuan 030024, PR China

ARTICLE INFO

This manuscript was handled by Huaming Guo, Editor-in-Chief, with the assistance of Fereidoun Rezanezhad, Associate Editor

Keywords:

Surface water
Inundation pattern
Remote sensing
Hydrodynamic model
Seasonal isolated lake
Poyang Lake

ABSTRACT

Determining the spatiotemporal dynamics of surface water in a heterogeneous floodplain is difficult, especially for its surrounding isolated lakes. Seasonal inundation patterns of these isolated lakes can be misestimated in a hydrodynamic model due to their short and erratic appearances. A surface water time series of Poyang Lake having an 8-day revisit frequency with a 30 m spatial resolution from 2000 to 2016 was conducted for the first time. This study was produced with a modified hierarchical spatiotemporal adaptive fusion model (HSTAFM) by integrating both Landsat and MODIS data. Discrepancies between model-based surface water and remotely-sensed surface water were evaluated, and possible causes were discussed. Results show that the modified HSTAFM can better detect the water features of a floodplain, thereby providing more detailed information in an seasonal isolated lake system than the MODIS MOD13Q1 product. With the fusion product, we found that Poyang Lake evidently shrank after experiencing a longer low-water period after the impoundment of the Three Gorges Dam. A large proportion of these discrepancies (averaging 36%) between model-based and remotely-sensed surface water distributed in seasonal isolated lakes, mainly occurred during high-water level periods. Uncertainties in the hydrodynamic model might attribute to smaller defined lake boundaries, bathymetric variations, human disturbance, and unconsidered groundwater recharge/discharge. These results provide a new insight into the temporally continuous and spatially dynamic assessment of simulated surface water, which is essential for the future improvement in the hydrodynamic model.

1. Introduction

Wetlands and other periodically inundated floodplains constitute a diverse ecosystem, which plays an important role in maintaining regional ecological and environmental functions including the hydrological cycle, biodiversity conservation, water quality protection and flood control (Acreman and Ferguson, 2010; Selwood et al., 2017). Unfortunately, terrestrial water bodies are undergoing a loss of biological diversity worldwide, which has been endangering the future of these ecosystems (Davidson, 2014; Winemiller et al., 2016; Zhang et al., 2017c). In general, the timing, extent, duration and variability of inundation affects vegetation development, wetland dynamics and ecosystem function maintenance (Casanova and Brock, 2000; Toogood and Joyce, 2009; Zhang et al., 2012; Tan et al., 2016). As a result, an accurate characterization of spatiotemporal variations in surface water is essential.

Mapping surface water changes has benefited a lot from the

accessibility of free remote sensing images, improved computational capacities and advanced image classification techniques. Such studies have largely filled the data gap over large remote and poorly gauged areas (Bates et al., 2014; Kuenzer et al., 2015; Pekel et al., 2016; Klein et al., 2017). Due to the lack of long-term (decades) synthetic aperture radar (SAR) data, optical sensors such as Landsat and MODerate-resolution Imaging Spectroradiometer (MODIS) are commonly used to capture surface water dynamics for large shallow water bodies over multi-decadal time periods (Jones et al., 2009; Hu et al., 2015; Tulbure et al., 2016; Huang et al., 2018).

At a 30-m resolution, Landsat sensors (onboard Landsat-4, 5, 7 and 8) have accumulated a large data pool since the 1980s, and have been widely used to monitor long-term surface water dynamics on both a global scale (Yamazaki et al., 2015; Pekel et al., 2016; Klein et al., 2017) and on regional scales (Rodrigues et al., 2012; Mueller et al., 2016; Jones et al., 2017). However, the 16-day satellite revisit cycle is generally not capable of detecting rapid surface changes, especially

* Corresponding author.

E-mail addresses: zqtan@niglas.ac.cn (Z. Tan), yunliangli@niglas.ac.cn (Y. Li), jyao@niglas.ac.cn (J. Yao), qzhang@niglas.ac.cn (Q. Zhang).

during wet and flood seasons (Frazier and Page, 2009; Jung et al., 2011). In addition, Terra and Aqua MODIS sensors have been used to study lake water variations (Feng et al., 2012; Khandelwal et al., 2017; Lu et al., 2017) and floodplain inundation (Islam et al., 2010; Huang et al., 2014; Heimhuber et al., 2018) due to their daily availability and broad spatial coverage. However, the coarse MODIS resolution (500 m MODIS data compared to 30 m Landsat data) is generally insufficient for capturing fragmented water bodies and inundation patterns within heterogeneous landscapes (Chen et al., 2013). Despite recent advances, there seems to be a trade-off between high spatial resolution and high temporal resolution for most current surface water records.

One feasible solution is to generate synthetic data through a combination of multi-sensor satellite data, such as those from Landsat and MODIS (Weng et al., 2014; Gao et al., 2015; Wu et al., 2016; Chen et al., 2017; Zhao et al., 2018). This solution can be realized using both indirect and direct strategies. The indirect strategy is to decompose coarse-scale MODIS observations using fine-scale Landsat observations. Based on this strategy, fusion models include the spatial and temporal adaptive reflectance fusion model (STARFM) (Gao et al., 2006), the semi-physical fusion approach (Roy et al., 2008), the spatial temporal adaptive algorithm for mapping reflectance change (STAARCH) (Hilker et al., 2009a, 2009b), the enhanced STARFM (ESTARFM) (Zhu et al., 2010), the spatial temporal data fusion approach (STDFA) (Wu et al., 2012), the multi-temporal fusion method (Amoros-Lopez et al., 2013) and the improved STDFA (ISTDFA) (Wu et al., 2016, 2018). These models use the relationship of reflectance between MODIS and Landsat data to predict Landsat-like reflectance at prediction dates. The limitations include: (1) lacking a pair of cloud-free images in humid regions (Michishita et al., 2015) and (2) assumption of no land cover change or only a linear change during the prediction period. These assumptions may not hold over rapidly changing land surfaces.

The direct strategy is to downscale normalized difference vegetation index (NDVI) data, which generally requires a fine-resolution auxiliary land cover/use database for pixel unmixing. Such models include the weighted linear mixing model (WLM) (Busetto et al., 2008), the spatial and temporal adaptive vegetation index fusion model (STAVFM) (Meng et al., 2013), the automated compound smoother (RMMEH) (Jin and Xu, 2013) and the NDVI linear mixing growth model (NDVI-LMGM) (Rao et al., 2015). These models are claimed to support the study of land surface dynamics in heterogeneous landscapes. Much like indirect methods, the direct methods also assume identical NDVI values for the same land use/cover type. This assumption may not hold within large areas where spectral heterogeneity is common even for the same land use/cover type. Therefore, an improved spatiotemporal fusion technique is required to address the above limitations.

For a seasonally inundated floodplain in the middle of the Yangtze River Basin, Poyang Lake hosts the most predominant ecosystem with free flow connections to the Yangtze River, and provides an ideal study site (Sun et al., 2012; Lai et al., 2014b). Dominated by gradual morphological changes, the extensive floodplain basin located on the flat landscape of the lake was segmented by complex levee systems and river channels. Many ecologically and economically important seasonal isolated lakes (sub-lakes) occur in these gradual floodplains along the western and southern lake offshores. These seasonal isolated lakes expand to a large surface water area during the flood period and shrink to a small area during the dry period (Shankman and Liang, 2003; Feng et al., 2012). When and where inundation occurs directly affects the wetland aquatic ecological conditions as well as irrigation and drinking water availability (Williamson et al., 2009; Ariztegui et al., 2010; Du et al., 2011).

Numerical modeling offers insights into inundation patterns. Physically based numerical models such as MIKE 21 (Li et al., 2014; Zhang et al., 2014; Yao et al., 2018), the coupled 1D and 2D hydrodynamic analysis model for the middle Yangtze River (CHAM-Yangtze) (Lai et al., 2014b), EFDC (Wang et al., 2015), Delft3D-FLOW (Zhang et al., 2017a), and GMS (Lan et al., 2015) have been established to

simulate the spatial distribution and temporal patterns of inundation at a large spatial scale. Despite the availability of digital elevation models plus extensive field surveys carried out in 1998 and 2010, the knowledge of this floodplain topography is still insufficient to model flood propagation. For seasonal isolated lakes, it is difficult to determine boundary conditions due to the complex flow patterns and limited *in situ* observations (Yao et al., 2018).

A number of pioneering studies have attempted to document the landscape changes of Poyang Lake using Landsat Thematic Mapper (TM)/Enhanced Thematic Mapper Plus (ETM+)/Operational Land Imager (OLI) data (Hui et al., 2008; Liu et al., 2013; Han et al., 2015), MODIS data (Feng et al., 2012, 2013; Wu and Liu, 2015; Cai et al., 2016), ENVISAT data (Andreoli et al., 2007; Xu et al., 2010; Liao et al., 2013), China's HuanJing (HJ) data (Zhao et al., 2011; Zhang et al., 2015) and microsatellite data (Dronova et al., 2011). However, it remains a challenge to capture rapid surface water changes with a fine spatiotemporal resolution, primarily due to the constraints on data availability. To address the above limitations, Chen et al. (2017) proposed a hierarchical spatiotemporal adaptive fusion model (HSTAFM) to produce synthetic NDVIs for surface water mapping. The fused NDVIs (2000–2014) had a 16-day revisit frequency at a 30-m spatial resolution. Comparisons based on observed images show that HSTAFM is more accurate than STARFM and FSDAF (Chen et al., 2018), but HSTAFM still requires validation over small seasonal isolated lakes and narrow river channels. In addition, the discrepancies between model and remote sensing derived surface water areas can be considerably large, despite Li et al. (2014) and Zhang et al. (2017b), who have shown good correlation between them. The knowledge gap of when, where and how model-remote sensing differences exist hampers their usage in various applications. Our study addresses this gap by integrating the novel time series of Landsat and MODIS data based on fulfilling the following two objectives:

- (1) To reconstruct the surface water series at 30-m and 8-day resolutions from 2000 to 2016, used for monitoring the rapid surface water changes of Poyang Lake, especially during rising and recession periods.
- (2) To investigate the discrepancies between and the uncertainties for surface water area derived from hydrodynamic modeling and remote sensing, especially in seasonal isolated lakes.

The method in this study provides a novel perspective for capturing surface water dynamics. It is expected to accommodate similar systems comprised of extensive floodplains and considerable water level fluctuations.

2. Study area

Poyang Lake is the largest lake in the Yangtze River basin. Controlled by an Eastern Asian monsoon, considerable seasonal water level variations (~10 m) create an extensive wetland ecosystem across a total area of approximately 3000 km² (Feng et al., 2013). A complex levee system (about 6400 km) has been built around the lake for flood protection (Shankman et al., 2006), leading to more than 77 seasonal isolated lakes during dry seasons when the lake is divided into many connected and disconnected segments separated by exposed floodplains (Fig. 1). These lakes range from 1 km² to over 71 km² in size, with a total surface water area of 767 km² and an average size of 10 km². For the Poyang Lake National Nature Reserve (PLNNR) and the Nanji Wetland National Nature Reserve (NWNNR), ~80% of the area is covered by these seasonal isolated lakes, which provide a wide range of foraging options for more than 80% of the migrating birds.

Water levels of seasonal isolated lakes increase as a result of continual inflow from five upstream tributaries (Xiushui, Ganjiang, Fuhe, Xinjiang and Raohe) and from the main lake during late spring and early summer (May and June). Most seasonal isolated lakes merge into

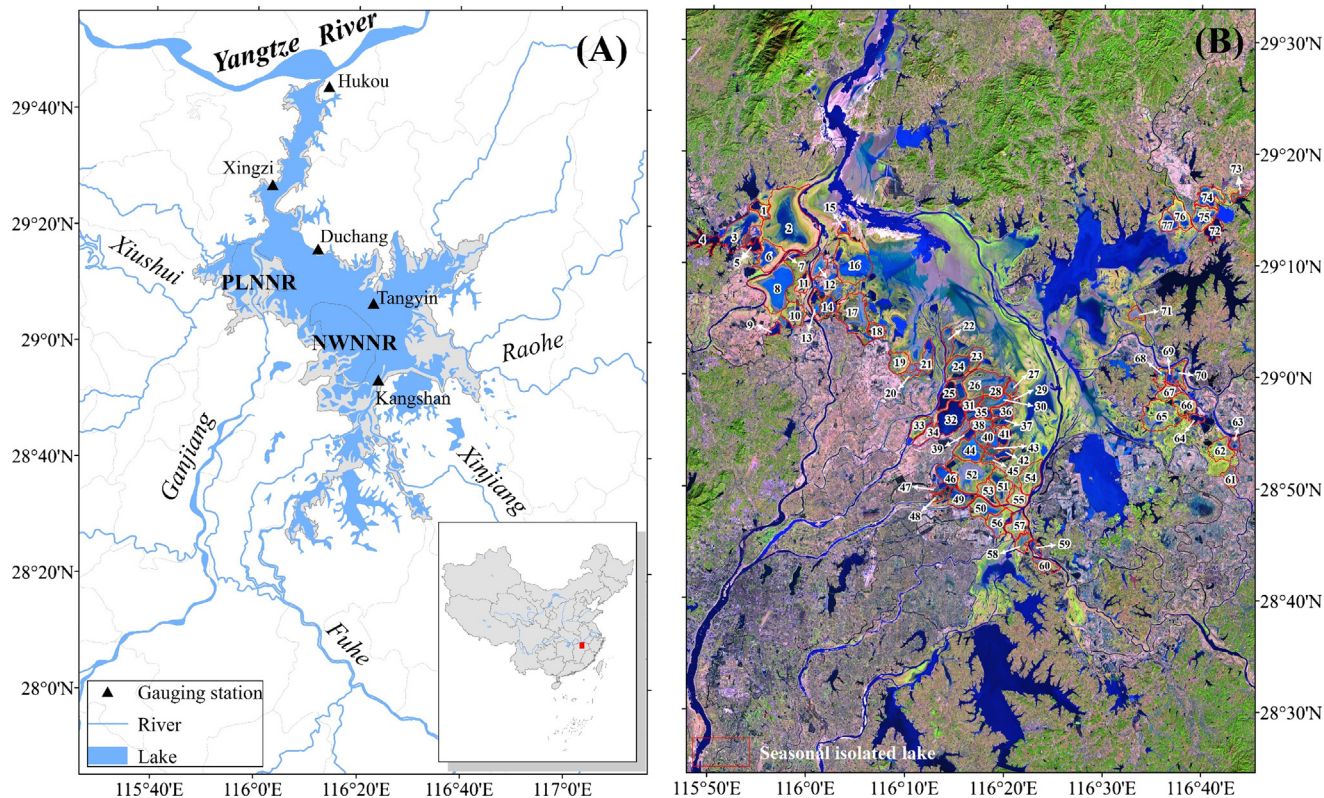


Fig. 1. (A) Location of the Poyang Lake and (B) distributions of 77 major seasonal isolated lakes (1. Zhoubianhu; 2. Banghu; 3. Niuyahu; 4. Nanhu; 5. Changhu; 6. Shahu; 7. Zhushihu; 8. Dahuichi; 9. Jihu; 10. Chizhouhu; 11. Changhuchi; 12. Zhonghuchi; 13. Xianghu; 14. Dongjiaihu; 15. Meixihu; 16. Dachahu; 17. Candouhu; 18. Xiaotanhuhu; 19. Dawuhu; 20. Chayegang; 21. Fanhu; 22. Caoyujiaohu; 23. Xiaduanhu; 24. Shangduanhu; 25. Mingxihu; 26. Nihu; 27. Xiaebeijia; 28. Hongxinghu; 29. Zhuhu; 30. Shangbeijia; 31. Bianhu; 32. Dashafanghu; 33. Liufanghu; 34. Shuanglinghu; 35. Dachehuang; 36. Beishenhu; 37. Nanshenhu; 38. Changhu; 39. Zhanbeihu; 40. Sanniwan; 41. Baishahu; 42. Shihu; 43. Shannanhu; 44. Sanhu; 45. Donghu; 46. Linchonghu; 47. Xihu; 48. Sanshuihu; 49. Ersihuihu; 50. Nanhu'; 51. Chengjiachi; 52. Liuliaohu; 53. Caowanhu; 54. Duzhouhu; 55. Jiyuhu; 56. Wangluohu; 57. Beikouwan; 58. Shatangchi; 59. Shangshuiwan; 60. Kanxiyahu; 61. Wanhu; 62. Beichahu; 63. Panhu; 64. Qijinhu; 65. Dalianzihu; 66. Beijiaohu; 67. Yunhu; 68. Siwanghu; 69. Beikouhu; 70. Nankouhu; 71. Shangganghu; 72. Jiaochahu; 73. Chatanghu; 74. Qihu; 75. Xuehu; 76. Dayehu; 77. Taiyanghu).

one single water body when the Yangtze River reaches its highest water level from July to early September. In late September, Poyang Lake starts receding again and most seasonal isolated lakes are disconnected and have differing water levels throughout the winter (from December to February). The timing and duration of floodplain exposure and inundation affects the wetland plant senescence and regeneration cycle, water quality and waterbird survival (Nishihiro et al., 2004; Liu et al., 2006; Raulings et al., 2010).

In recent years, Poyang Lake has experienced significant changes due to intensive anthropogenic activity and climate change. Construction of the Three Gorges Dam (TGD), which began to impound water in 2003 arguably has had the largest impact on flow and sediment regimes (Fang et al., 2012). Since the TGD came into operation, the inundation pattern and the distribution of wetland habitats in floodplains has changed dramatically (Guo et al., 2012; Zhao et al., 2013; Mei et al., 2016), which in turn has had detrimental impacts on its ecological function as a habitat for fish (Turvey et al., 2010) and waterbirds (Barzen et al., 2009). In addition, Liu et al., (2013) revealed that the lake change was a synthetic result of precipitation, evapotranspiration, and outflow discharge. However, the natural dynamics of surface water in numerous temporal and widespread seasonal isolated lakes remains unclear.

3. Methods

3.1. MODIS data and pre-processing

The 250-m resolution 8-day composited MOD13Q1 data (tile no.

h28v06) in 2000–2016 were obtained from the National Aeronautics and Space Administration (NASA) Earth Observing System Data and Information System (EOSDIS) ([url: https://lpdaac.usgs.gov/data_access/data_pool](https://lpdaac.usgs.gov/data_access/data_pool)). A constrained view angle-maximum value composite (CV-MVC) and a bidirectional reflectance distribution function (BRDF) algorithm have been designed to filter out the effects of instrument calibration, sun angle differences, terrain, cloud shadows and atmospheric conditions (Jin and Xu, 2013; Michishita et al., 2014). Furthermore, the running median, mean value, maximum operation, end point processing and hanning (RMMEH) smoothing method (Jin and Xu, 2013) was adopted to reduce the residual noise of the NDVI profile and to reconstruct a high quality NDVI time series. The dataset was then blended with Landsat images to produce a dense and fine-resolution NDVI time-series. Fig. 2 shows all the MODIS and Landsat data used in our study.

3.2. Landsat data and pre-processing

A total of 129 cloud-free Landsat TM, ETM + and OLI (at a spatial resolution of 30 m) images were downloaded from the United States Geological Survey (USGS) ([url: http://www.usgs.gov/](http://www.usgs.gov/)). These images were first converted to top-of atmosphere (ToA) radiance using radiometric calibration coefficients in the metadata files. Then, the FLAASH (Fast Line-of-sight Atmospheric Analysis of Spectral Hypercubes) module embedded in ENVI 5.1 software was used to generate surface reflectance data. To fill the gaps present in ETM + images after May 31, 2003, the triangulation method developed by Scaramuzza et al. (2004) was applied. Finally, Landsat NDVI and normalized difference water

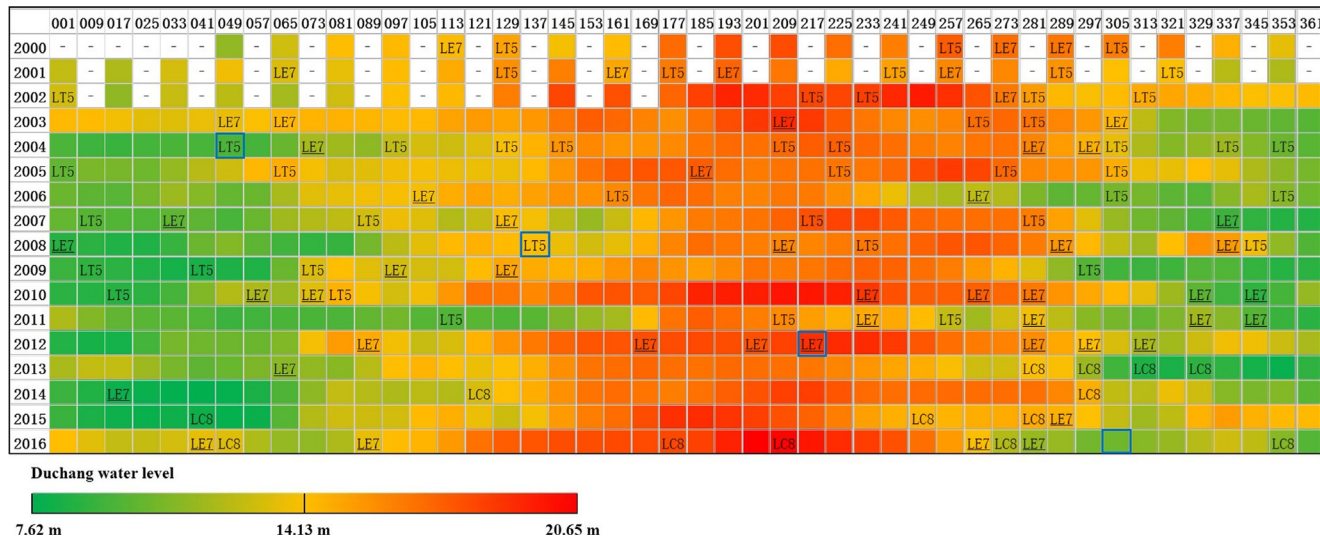


Fig. 2. Temporal distribution of Landsat (TM/ETM + /OLI) and MODIS data acquired in this study for Poyang Lake. Vertical axis denotes years from 2000 to 2016, and horizontal axis denotes day of year (DOY). Colored cells labeled with LT5 present Landsat-5 TM data, LE7s present Landsat-7 ETM+ data and LC8s present Landsat-8 OLI data. Underlined LE7s present SLC-off data after May 31, 2003. Blue boxes point out four samples for visual inspection. Each cell of the matrix color-coded represents different water levels at Duchang station. (For interpretation of the references to color in this figure legend, the reader is referred to the web version of this article.)

index (NDWI) images were calculated using the reflectance data.

3.3. Hydrodynamic modeling data and pre-processing

In this study, remote sensing-based surface water results were compared to model-based results. The inundation depth of Poyang Lake (2000–2012) was simulated by the MIKE 21 model (DHI, 2007), which is a 2D depth-averaged hydrodynamic model implemented previously by Li et al. (2014). The model defines a total lake area of 3124 km² according to historical lake surface areas during periods with high water levels. A 2D grid system with an unstructured triangular grid was adopted to capture the complex bathymetry of Poyang Lake (surveyed in 1998 and updated in 2000). The edge length of mesh elements varied from 70 to 1500 m, resulting in a total of 20,450 triangular elements. The time step was set to 5 s to limit the Courant-Friedrich-Levy (CFL) number for a stable solution. Because groundwater observations and geological data are not available, no attempts were made to simulate groundwater dynamics. A detailed description of the model can be found in our former studies (Tan et al., 2016; Zhang et al., 2017b). Finally, daily time series data were averaged to 16-day (Jan. 1, 2000 to Jun. 26, 2002) and 8-day (Jun. 27, 2002 to Dec. 31, 2016) time steps.

3.4. Generating synthetic 8-day Landsat NDVI images using HSTAFM

The HSTAFM model proposed by Chen et al. (2017) was applied in this study. Compared to the STARFM-like fusion models, the featured improvement of HSTAFM is the introduction of an initial prediction and integration of that initial prediction into a hierarchical strategy for selecting similar pixels. The improvement can best capture land surface changes within the limited available prior/posterior Landsat-MODIS image pair and targeted MODIS image.

Four steps were followed to implement the HSTAFM approach. First, MODIS data were reprojected and resampled according to Landsat images. Second, an initial predicted fine resolution image was produced using a direct multiplier method. Third, a hierarchical “similar pixels” scheme was used to identify both prior (or posterior) and predicted dates. Fourth, a weight W_{ij} (Eq. (1)) was assigned to each similar pixel based on: (i) the spectral difference (s_{ij}) between NDVI of the base Landsat-MODIS image pair and (ii) the spatial Euclidean distance (d_{ij}) between the neighbor and the central pixel. Fifth, the NDVI value of the

central pixel was computed with the algorithm characterized in Eq. (1):

$$F_2(x_{\omega/2}, y_{\omega/2}, b) = \sum_{i=1}^{\omega} \sum_{j=1}^{\omega} W_{ij} * P_{ij} * [L_1(x_i, y_j, b) + M_2(x_i, y_j, b) - M_1(x_i, y_j, b)] \quad (1)$$

$$W_{ij} = \frac{1/(s_{ij} * d_{ij})}{\sum_{i=1}^{\omega} \sum_{j=1}^{\omega} 1/(s_{ij} * d_{ij})} \quad (2)$$

$$s_{ij} = \frac{P_{ij} * |L(x_i, y_j) - L(x_{\omega/2}, y_{\omega/2})|}{\sum_{i=1}^{\omega} \sum_{j=1}^{\omega} P_{ij} * |L(x_i, y_j) - L(x_{\omega/2}, y_{\omega/2})|} \quad (3)$$

$$d_{ij} = 1 + \sqrt{(x_i - x_{\omega/2})^2 + (y_j - y_{\omega/2})^2} / (1 + \omega) \quad (4)$$

where ω denotes the moving window size; W_{ij} is the combined weight determined by the spectral and distance differences according to Eqs. (2)–(4), and P is the similar pixel set represented by a binary matrix. A more detailed description of the HSTAFM algorithm can be found in two previous papers by Chen et al. (2017, 2018).

In this study, contemporary MODIS and Landsat images (observed in the same year) with the most similar land surface information were chosen to make up a pair. The water level data at the Duchang station served as a reference. If the contemporary criterion was not met, another Landsat image with the closest water level and phenological period in the previous or next year was chosen as an alternative.

3.5. Surface water extraction using the Jenks natural breaks method

The Poyang Lake is mainly covered by dense vegetation (Tan et al., 2016); therefore, the fused NDVIs were classified as water and non-water classes. In this study, the Jenks natural breaks method, also called the Jenks optimization method, is a data clustering method used to find existing groups of values, which are then joined together to exploit natural gaps in the data (Jenks, 1977). Class breaks are identified based on their ability to best group similar values and maximize the differences between classes. The input data are divided into classes, and their boundaries are set where relatively large differences exist between data values (Carr et al., 2002).

Three main steps were followed to implement the Jenks (1967, 1977) natural breaks: Step 1: Calculate the “sum of squared deviations

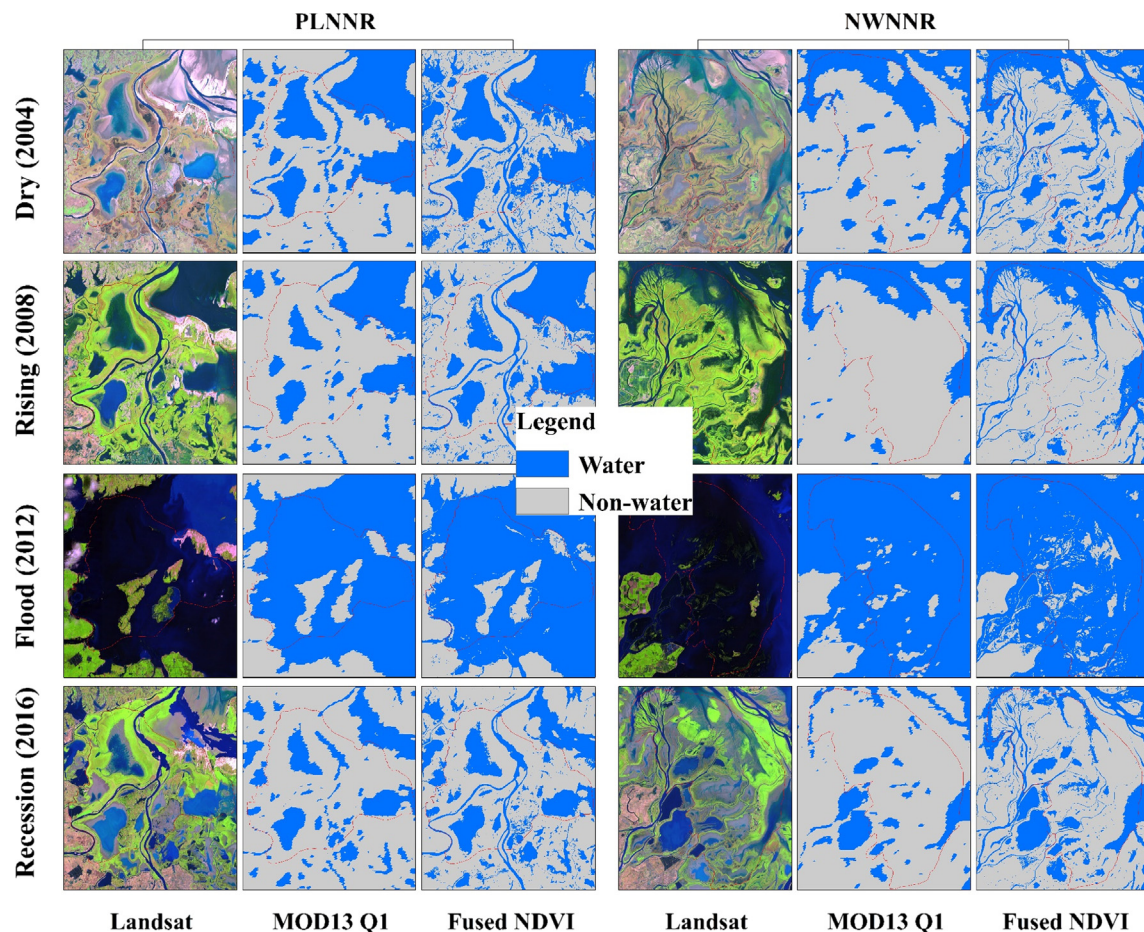


Fig. 3. Comparison of spatial details between MOD13Q1 products and fused NDVIs from the HSTAFM on February 18, 2004 (DOY: 49), May 16, 2008 (DOY: 137), August 4, 2012 (DOY: 217) and December 16, 2016 (DOY: 353).

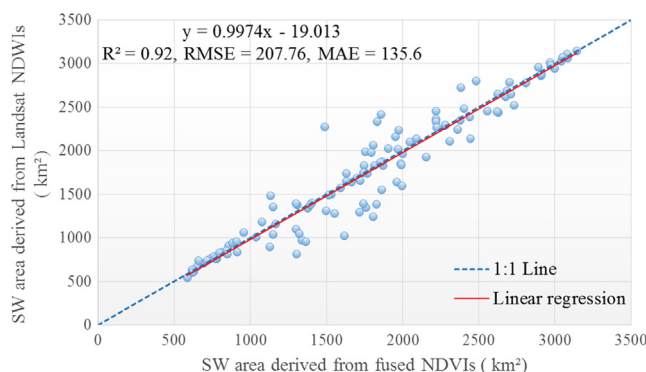


Fig. 4. Relationships between water surface areas derived from fused NDVIs and Landsat NDWIs. Solid line indicate the best fit between the two datasets, and 1:1 dashed line is a diagonal line representing a perfect match.

for array mean” (SDAM). Step 2: For each range combination, calculate the “sum of squared deviations for class means” (SCDM_ALL), and find the smallest one. SCDM_ALL is much like SDAM, but uses class means and deviations. Figure out the smallest SCDM_ALL, so its “best ranges” minimize the variations within classes. Step 3: Calculate a “goodness of variance fit” (GVF), defined as $(SDAM - SCDM)/SDAM$. GVF ranges from 1 (perfect fit) to 0 (awful fit). The higher SCDM_ALL (more variation within classes) results in a lower GVF.

4. Results

4.1. Blended surface water series and its accuracy

Based on the fused NDVIs, surface water mapping was performed using Jenks natural breaks method. To demonstrate the performance of this surface water result, visual interpretation was performed in the PLNNR and NWNNR for different hydrological periods using a uniform sampling strategy (Fig. 3). Samples without an available Landsat image on Oct. 31, 2016 (Day of Year, DOY: 305) were replaced by images obtained on Dec. 16, 2016 (DOY: 353).

The blended 30-m surface water series accurately discerns small water bodies in the two national reserves. Because of the coarse MODIS spatial resolution, shallow water can be misclassified and confused with muddy sediment. As shown in Fig. 3, the surface water derived from fused NDVIs performs better in detecting the boundaries of small seasonal isolated lakes. Meanwhile, the spatial continuity of the narrow rivers was maintained on the blended surface water maps, especially during low water level periods. Surface water area data derived from fused NDVIs show a high correlation with those derived from Landsat NDWI ($R^2 = 0.92$), demonstrating that the former has a similar accuracy compared with the high spatial resolution images (Fig. 4). The root mean square error (RMSE) between the two series is 208 km², and the mean absolute error (MAE) is 136 km².

Poyang Lake and its seasonal isolated lakes show strong seasonality in their surface water areas. The annual maximum surface water (3153 km²) of the whole lake occurred on Jul. 19, 2016 (DOY: 201), and the minimum surface water (555 km²) occurred on Jan. 17, 2004 (DOY: 017). For all seasonal isolated lakes, the maximum surface water

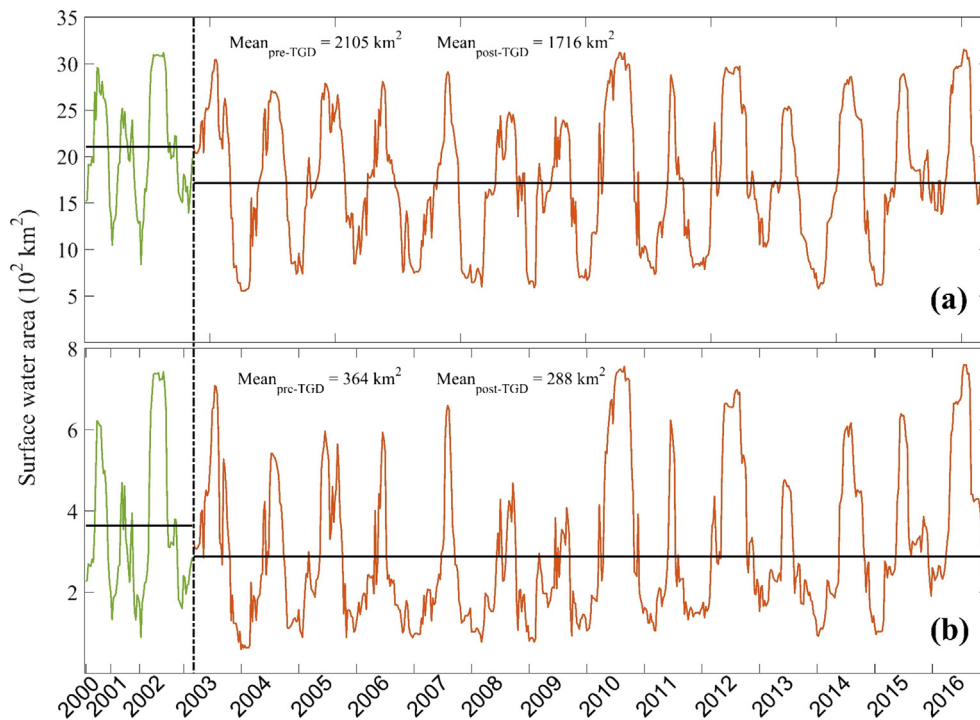


Fig. 5. Variations of surface water area for (a) the whole Poyang Lake and (b) seasonal isolated lakes between 2000 and 2016. Green lines present surface water areas before the impoundment of TGD (pre-TGD), and red lines present surface water areas after the impoundment of TGD (post-TGD). A black solid line presents the mean surface area during each period (hydrological year). (For interpretation of the references to color in this figure legend, the reader is referred to the web version of this article.)

(760 km²) was found on Jul. 27, 2016 (DOY: 209) and the minimum surface water (59 km²) was found on Jan. 1, 2004 (DOY: 001). The annual maximum/minimum surface water ratio ranged from 2.0 to 4.9 for the whole lake and from 2.8 to 9.2 for all seasonal isolated lakes.

Specifically, the whole Poyang Lake showed a mean surface water area of $2105 \pm 595 \text{ km}^2$ in the pre-TGD period (2000–2002, hydrological year), which decreased by 389 km^2 to $1716 \pm 716 \text{ km}^2$ during the post-TGD period (2003–2016, hydrological year) (see Fig. 5). The difference between the two periods is statistically significant (ANOVA, $p < 0.05$). The striking results of the significant decrease in surface water areas after the impoundment of TGD were consistent with former studies (Feng et al., 2013). In comparison, although a decrease of surface water area (from $364 \pm 190 \text{ km}^2$ to $288 \pm 173 \text{ km}^2$) was also found in seasonal isolated lakes after the impoundment of TGD, the differences between the two periods were not significant ($p > 0.05$).

The decreasing trends in the long-term surface water area for both the whole Poyang Lake and seasonal isolated lakes were further revealed by variations in the duration of the low-water period during each year (Fig. 6). The duration of the low-water period was derived from the number of surface water map with areas that were below the

mean surface water area of the dry season (from December to February) between 2000 and 2015. Approximately, the much shorter duration of low-water periods ranged from 0 to 8 days (1×8 days) for the whole lake and 0 to 24 days for the seasonal isolated lakes during the pre-TGD period, leading to a general but not significant trends (3.12 days per year and 0.16 days per year, respectively) in the long-term variations. To be specific, the longest low-water periods were observed in the hydrological year of 2007 for both the whole lake (144 days) and seasonal isolated lakes (144 days). Notably, the moderate shrinkage of the whole Poyang Lake and seasonal isolated lakes was mainly caused by the earlier dry season starting dates. Meanwhile, the serious shrinkage of the lake was caused by both the earlier starting dates and the later ending dates of the dry seasons.

4.2. Comparison of remotely-sensed and model-based surface water

In this study, a spatiotemporal comparison of surface water derived from a hydrodynamic model (MIKE 21) with fused NDVIs (from the HSTAFM) was tested to better identify errors and, hence, make improvements to either or both of these datasets. Temporal profiles of remotely-sensed surface water areas and model-based surface water areas from 2000 to 2012 are displayed in Fig. 7. However, the model-based surface water profile after 2012 is not shown in Fig. 7 due to lack of basic data. The temporal variation and changing trend for the whole lake and seasonal isolated lakes achieved a general high consistency between these two datasets, suggesting that both methods could successfully capture the inundation dynamics of the study area most of the time. However, the consistency varied from year to year. For the whole Poyang Lake, the most significant discrepancy of the surface water area appeared in 2008, with an average difference of 364 km^2 . Meanwhile, the minimum difference was 164 km^2 on average, which was detected in 2010. Like the whole Poyang Lake, the maximum and minimum surface water differences of seasonal isolated lakes between these two datasets were also detected in 2008 (128 km^2) and 2011 (51 km^2). For the whole period, area differences between remotely-sensed surface water and model-based surface water ranged from 2 km^2 to 1045 km^2 (on average, 264 km^2) for the whole lake, and from 0 km^2 to 412 km^2 (on average, 83 km^2) for seasonal isolated lakes. In addition, the

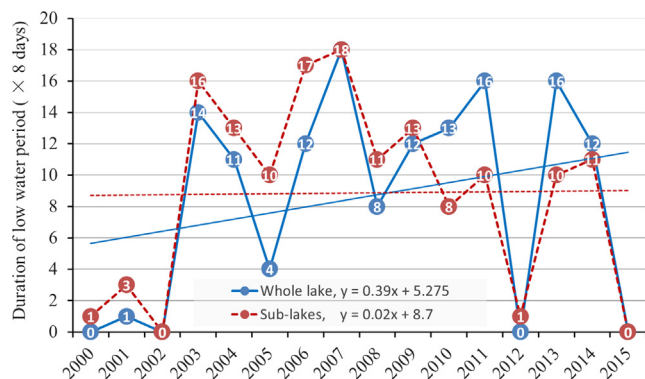


Fig. 6. Durations of low-water period between 2000 and 2015. Labeled numbers present the number of scenes having surface water areas smaller than mean values during dry seasons. One scene presents 8 days.

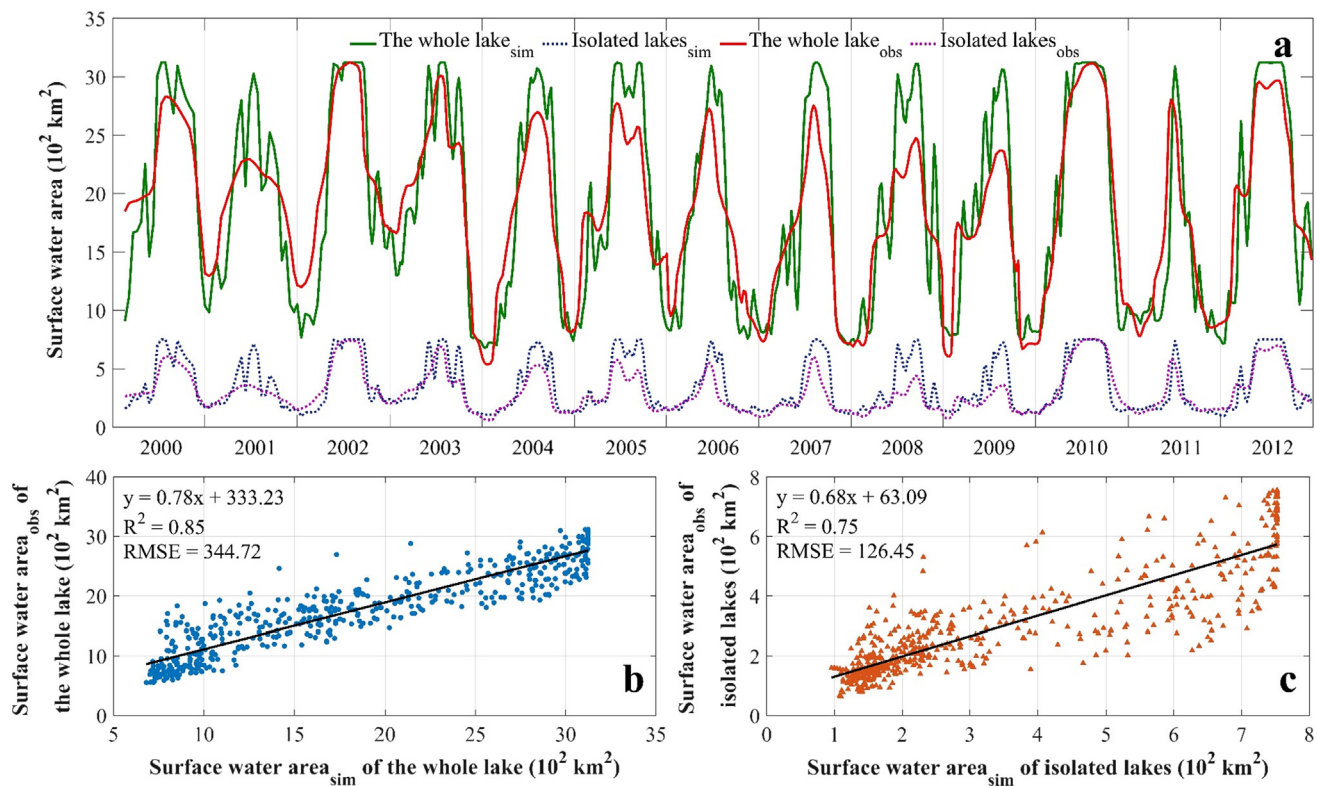


Fig. 7. Remotely-sensed (obs) and model-based (sim) surface water area during 2000–2012. (a) Presents the surface water area of the whole Poyang Lake and seasonal isolated lakes derived from fused NDVIs and hydrodynamic model, respectively. (b) Shows the relationship between remotely-sensed and model-based surface water areas for the whole Poyang Lake. (c) Shows the relationship between remotely-sensed and model-based surface water areas for seasonal isolated lakes.

relationship between remotely-sensed surface water and model-based surface water for the whole lake ($R^2 = 0.85$) is better than that for seasonal isolated lakes ($R^2 = 0.75$) as shown in Fig. 7b and Fig. 7c, respectively. In the whole Poyang Lake, an overall 36% difference between remotely-sensed surface water and model-based surface water was attributed to estimation errors for seasonal isolated lakes. Notably, the maximum areas of the model-based surface water were constant during different years for both the whole lake (3124 km^2) and seasonal isolated lakes (752 km^2).

An annual bias estimation for seasonal isolated lakes is further recognized in Fig. 8, which shows the monthly average differences between areas of remotely-sensed surface water and areas of model-based surface water varying from 1 km^2 to 164 km^2 (Fig. 8a). The model-remote sensing discrepancies were much larger in July (164 km^2), August (129 km^2), and September (153 km^2) than in other months. On the seasonal variations, the average area of model-based surface water (481 km^2) was much larger than the remotely-sensed surface water (756 km^2) (Fig. 8b). Contrary to the considerable discrepancy during the flood period, the remotely-sensed surface water and model-based surface water matched each other well during rising periods (with a difference in the average surface water area of 17 km^2), recession periods (with a difference in the average surface water area of 63 km^2), and dry periods (with a difference in the average surface water area of 10 km^2).

In previous studies on Poyang Lake and the middle and lower reaches of the Yangtze River, 2006 was frequently analyzed as a typical drought year (Dai et al., 2008; Li et al., 2017), and 2010 was recognized as a typical flood year (Feng et al., 2012). Fig. 9 highlights the relationship between remotely-sensed surface water areas and model-based surface water areas in typical years. As shown in Fig. 9, the surface water areas derived from model achieved the best consistency to the surface water areas derived from remote sensing in a typical flood year (with a coefficient of correlation $R^2 = 0.92$), which was

better than the consistency achieved in the normal year ($R^2 = 0.86$) and in the typical drought year ($R^2 = 0.66$). In Fig. 9b, most points distributed above the 1:1 line, indicate that the hydrodynamic model always overestimates the surface water area in a drought year, especially during the flood period.

5. Discussion

Large lakes like the Poyang Lake typically form wide floodplains occupied by seasonal isolated lakes, streams, rivers, and wetlands. The correlation between the inundation area of a lake or wetland and nearby river water level fluctuations can be presumed indicative of hydrological connectivity between the river main-stem and its surrounding floodplain. Hydrological connectivity is important not only for the floodplain morphogenesis and system maintenance, but for nutrient recycling among biotas. Monitoring the hydrological connectivity demands more continuous (both spatial and temporal) records of inundation dynamics taking place over the floodplain. As a cost-effective approach, spatiotemporal fusion techniques have proved useful in monitoring the dynamics of phenology. However, some emerging problems remain. For example, the STARFM-like methods cannot deal with transient disturbance or land cover change situations, because these methods require the primary assumption that “the land cover type does not change between the baseline and predicted dates” (Chen et al., 2018). In this study, the modified HSTAFM method can better capture the general change between the prior/posterior and predicted dates, and it offers an efficient tool to monitor the dynamics of deltaic systems, especially of small seasonal isolated lakes and narrow river channels.

In addition, this paper investigates in more detail the discrepancies between remotely-sensed and model-based surface water series. The authors deemed that the hydrodynamic modeling approach appears to be limited in this case study, especially in the simulation of seasonal

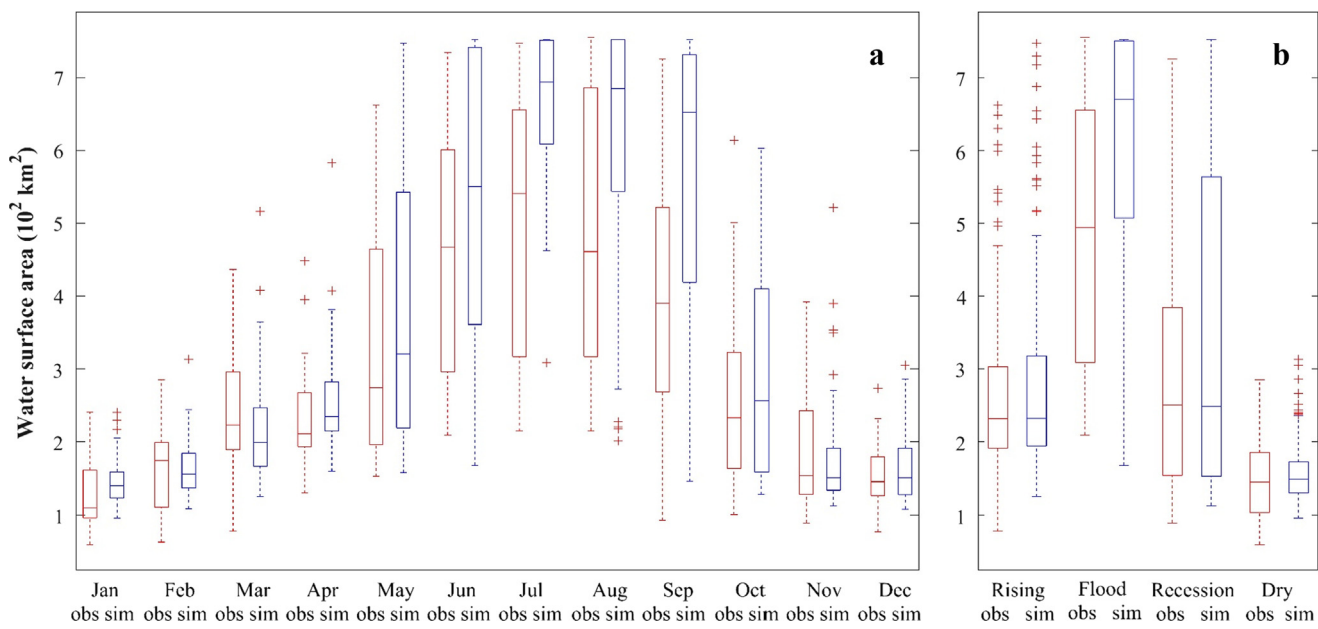


Fig. 8. (a) Monthly and (b) seasonal changes of surface water area of seasonal isolated lakes.

isolated lakes. Karim et al. (2011) estimated floodplain inundation in the Fitzroy River catchment using hydrodynamic modeling and remote sensing. They found that simulated inundations are large compared with MODIS detected inundations, and the difference is larger at the later flood stage. The author proposed that potential sources of model error are (1) the use of large grids to reproduce steam channels; (2) implementation of a “steady state” initial condition and (3) use of a simplified land use map to estimate land surface roughness.

The first limitation also exists in this study. Considering the model's stability and efficiency, the edge length of mesh elements varied from 70 to 1500 m for different lake topographies at different scales. These elements were coarser on flat alluvial plains and finer in deep rivers and channels. Compared to remote sensing data, hydrodynamic models usually have coarse meshes, which cannot effectively capture the terrain differences and bathymetric changes. These simulation uncertainties were amplified in the simulations of low-gradient floodplains in the southern and western shores of Poyang Lake, where most seasonal isolated lakes are distributed. Besides, since 2000, the bed elevation of the Hukou outflow channel has decreased significantly due

to intensive illegal sand mining activities (de Leeuw et al., 2010; Lai et al., 2014a). Lai et al., (2014a) proved that despite the sand mining activities, which usually occurred in the northern channels, the discharge ability of Poyang Lake into the Yangtze River during the dry season increased 1.5–2 times due to bathymetric changes. Yao et al., (2018) proposed that the bed erosion of the northern outlet channel averaged 3 m, resulting in a decrease in the water level by 1.2–2 m in the most significant influence areas. Hydrodynamic models based on historical digital elevation models (DEMs) may have produced deviations in simulations years ago or later.

As for the second limitation in Karim's model, the initial conditions in this model were obtained by interpolating the observed surface water elevations at the five gauging stations. Additionally, based on the object-oriented classification, spatially varying Manning's roughness coefficients were derived from the empirical parameters of landcover types with high spatial resolution. Thus, the third limitation in Karim's model cannot be a critical factor causing simulation error in this study. Given the considerations discussed above, there are some other limitations causing simulation uncertainties that need attention.

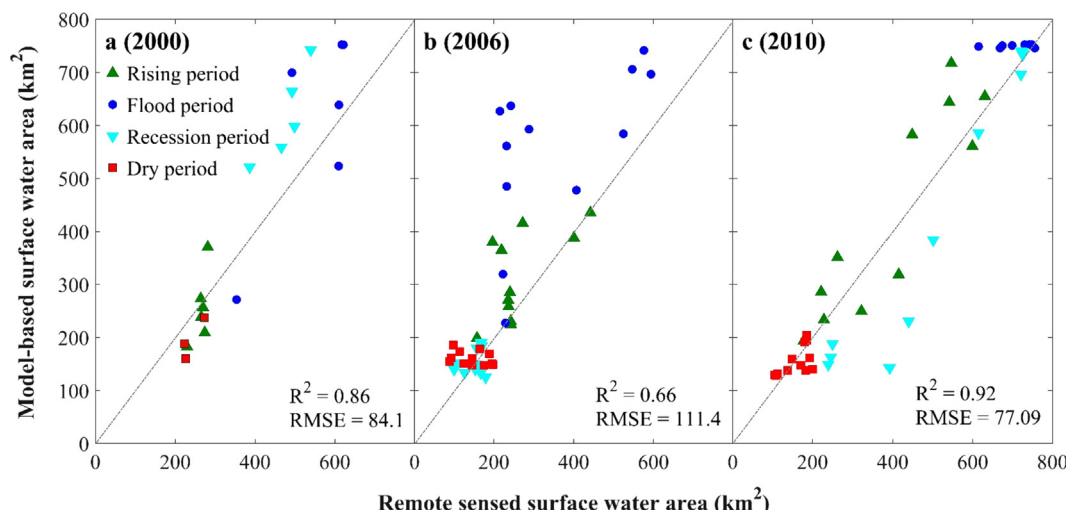


Fig. 9. Relationships between remotely-sensed and model-based surface water area for seasonal isolated lakes during (a) the normal year, (b) the typical drought year and (c) the typical flooding year.

First, the model boundary in this study is not the same as the real one. Poyang Lake is historically a region of significant floods. Extensive levee-building began after the 1954 floods. Before 1950, the total length of levees in Jiangxi was about 3100 km. The levee system was made higher and wider in the 1950s. In the 1970s, land was reclaimed from the Poyang Lake, but after the 1998 flood, farmlands destroyed by war and floods during the late 1800s and early 1900s were returned to the lake. There are now 6400 km of levees that provide protection to 10,000 km² of farmland and to a population of about 10 million people who live in the low-lying areas at the margins of Poyang Lake (Shankman and Liang, 2003). The levees have been continuously improved. A complex levee system and its dramatic changes make it difficult to confirm the actual boundary of Poyang Lake, which is important when modeling. In this study, an area of 3124 km² was determined by examining the historic flood event in 1998, which was smaller than the Poyang Lake area described in other literature (Shankman et al., 2012). Because the northern channel connected to the Yangtze River is Poyang Lake's only outlet, the discharge capability of the lake is constrained by the locking effect of the Yangtze River. Continuous rising of the high-water level will result in rising depths of inundation regions, but the surface water area will remain static after reaching its maximum value. This may account for the stable surface water that occurred in the model during the flood period.

Second, the inundation patterns of some seasonal isolated lakes are disturbed by human activities. To the best of our knowledge, at least 22 seasonal isolated lakes have water levels that are manipulated by independent control gates. Their elevations at central points and at bottom elevations of control gates are listed in Table 1. These lakes have been contracted to local fishermen for fishing and planting. Control gates are usually closed in the early recession period to maintain water for fish growth and then opened in January for harvest. However, the closed and open time of the control gates differ. It is almost impossible to accurately simulate the inundation patterns of all seasonal isolated lakes without any regulation information record.

Third, subsurface hydrological processes are not considered in this model. One of our former studies (Li et al., 2018) revealed that the groundwater level variations of a typical wetland in PLNNR were sensitive to the lake water level fluctuations, with a correlation coefficient varying from 0.93 to 0.99 between them. Based on the records of more than 40 groundwater observation wells in Poyang Lake Basin, Lan et al. (2015) confirmed that about 53.3% correlation coefficients between

groundwater levels and nearby river levels were larger than 0.90, and 93.3% of these correlation coefficients were larger than 0.80, suggesting the presence of a good underground hydrological connectivity. However, for seasonal isolated lakes, the groundwater discharge/recharge has been neglected in hydrodynamic models, which only consider the impact of precipitation and evaporation when these lakes "disconnect" from each other or the main lake. This insufficiency of the hydrodynamic model may cause an underestimation of surface water for seasonal isolated lakes during a water-rising period, and an overestimation during a water-recession period.

Although the remote sensing approach performed better than the hydrodynamic modeling approach in this study, the abilities and challenges of using optical remote sensing, especially the fusion model, needs further discussion. Three significant limitations in the remote sensing approach can be summarized as follows.

First, water under a vegetation canopy is easily misclassified. A challenge for remote sensing of inundated floodplains is the capacity to identify water under vegetation canopies, including both emerging and floating macrophyte canopies. Flooded vegetation and soil formed a transition area of mixed pixels between water, flooded wetland vegetation, dry land vegetation and bare ground soil, occurring on the edges of open water. Optical remote sensing technologies provide a wide coverage at a range of spatial and spectral resolutions but have limitations when covering tropical floodplains because the surface water is often obscured by dense overlying vegetation. To understand spatio-temporal inundation patterns of floodplains, one must first understand the development of a time series of inter-annual and seasonal maps of variability in flooded standing vegetation. Thus, longer wavelength (L-band) synthetic aperture radar (SAR) data have become the preferred data source because of the capacity of L-band data to detect water under some canopies (Evans et al., 2010; Ward et al., 2014). The fusion of microwave (L-band SAR) and optical (Landsat TM 5) satellite data provides us with a new insight to capturing the complex seasonal dynamics of floodplain aquatic vegetation cover and inundation.

Second, discrepancies exist in Landsat-MODIS pairs. Limitations remain in the HSTAFM method, including errors produced by minor changes occurring at sub-pixel resolution and errors introduced by the predicted images in selecting final similar pixels. This problem was clarified by Chen et al. (2018). In their fusion model, the accuracy of the final predicted image depended on the accuracy of the initial predicted NDVI value with Landsat-like spatial resolution at the target date. Meanwhile, the initial predicted fine-resolution NDVI (L_2) was calculated from the observed MODIS NDVI value at the target date (M_2) and the observed NDVI value of MODIS (M_1) and Landsat (L_1) at a prior or posterior date by $L_2 = L_1 \cdot M_2 / M_1$, assuming that L_1 was consistent with M_1 . In this study, despite variations, water levels and phenology were considered to reduce the difference between L_1 and M_1 as far as possible; however, land cover changes still exist due to the lack of available Landsat images. The discrepancy between M_1 and L_1 , which was observed in different years, may lead to an aggregation of change detection biases in the final prediction. Other optical data with fine spatial resolution, such as Sentinel-2 and GaoFen-3 may be helpful to fill the gap of data shortages, especially in recent years.

Third, the best threshold for index varies in space and time. Temporal dynamic thresholds were adopted for determining the optimal value in order to distinguish water bodies and non-water bodies from differing conditions or sensor differences. However, an ideal single threshold for water or vegetation indices is difficult to determine because the spectral signature of water varies both in time and space (Tulbure et al., 2016). Therefore, threshold definition in one image must also be considered in the context of intrinsic water characteristics and the land cover complexity of distinct regions.

As discussed above, uncertainties in hydrodynamic modeling and remote sensing inhibit its use in flood mapping. Interest in integrating these two fields has increased with the availability of remote sensing data which are freely available near-global and frequent. For example,

Table 1
Manipulated isolated lakes and their elevations.

ID	Isolated lake	Elevation of central point (m, MSL)	Bottom elevation of control gate (m)
2	Banghu	11.00	9.75
6	Shahu	12.50	11.03
7	Zhushihu	12.50	11.53
8	Dahuchi	12.00	10.34
11	Changhuchi	12.04	11.39
12	Zhonghuchi	12.50	11.24
13	Xianghu	13.30	11.55
15	Meixihu	13.00	11.20
24	Shangduanhу	12.80	11.84
26	Nihu	12.60	11.37
27	Xiabeijia	12.50	11.56
29	Zhuhu	13.16	12.18
30	Shangbeijia	12.95	11.35
35	Dachehuang	13.80	11.82
36	Beishenhu	12.66	11.59
37	Nanshenhu	12.50	11.81
38	Changhu	12.50	12.04
39	Zhanbeihu	13.10	12.35
40	Sannianwan	13.10	12.06
41	Baishahu	11.80	11.54
42	Shihu	12.10	11.57
58	Shatangchi	12.6	11.66

Karim et al. (2011) found that the availability of remotely-sensed flood inundation maps was very useful for model calibration. Moreover, Ticehurst et al. (2015) improved the mapping of flood events based on the daily MODIS Open Water Likelihood algorithm by successfully using information from the hydrodynamic model. We believe, in the near future, the combination of hydrodynamic modeling and remote sensing will provide a useful way for assessing flood discharge and the duration and frequency of wetland connectivity for broad-scale water resource assessment.

6. Conclusions

A remotely-sensed surface water series with an 8-day revisit frequency at a 30 m spatial resolution from 2000 to 2016 was first produced in Poyang Lake using the modified HSTAFM method. A total of 129 surface water maps extracted from cloud-free Landsat NDWIs were applied to evaluate the performance of the fusion method, verifying that it can be reasonably employed in monitoring rapidly varying floodplains. With the analysis of the blended surface water series, we found that the annual average area of surface water decreased evidently after the operation of the TGD, both for the whole Poyang Lake and seasonal isolated lakes. The duration of the low-water period increased between 2000 and 2015, with a changing rate that was higher for the whole lake than for seasonal isolated lakes.

As a major step forward, this research quantifies the temporal and spatial variations of discrepancies between model-based surface water and remotely-sensed surface water. A relatively higher correlation between these two datasets was found for the whole lake, especially during low-water level periods. On average, overall discrepancies of 36% were found in regions covered by seasonal isolated lakes and occurred more often during the flood period. Moreover, it was found that the simulated surface water matched the observed surface water best in the typical flood year and worst in the typical drought year. Constraint of the designed model boundaries and influences of varied bathymetry might limit the simulation accuracy. Manipulation of seasonal isolated lakes could proportionally contribute to subsequent simulation uncertainties. Additionally, groundwater discharge and recharge should be taken into consideration in further simulations.

This work presented the temporally continuous and spatially dynamic surface water of Poyang Lake, providing new insight into the uncertainties of the hydrodynamic model and remote sensing. Given the rapid changes of the inundation pattern in Poyang Lake, the 8-day interval of the remotely-sensed surface water data collection still seems coarse. Despite lots of uncertainties identified while applying the hydrodynamic model during this study, it remains a powerful tool for identifying continuous spatiotemporal changes in complex floodplain systems.

Declaration of interest statement

We declare that we have no financial and personal relationships with other people or organizations that can inappropriately influence our work, there is no professional or other personal interest of any nature or kind in any product, service and/or company that could be construed as influencing the position presented in, or the review of, the manuscript entitled “Mapping Inundation Dynamics in a Heterogeneous Floodplain: Insights from Integrating Observation and Modelling Approach” (HYDROL29903).

Acknowledgements

We appreciate Bin Chen for providing the fusion model code and for his willingness to share his knowledge and expertise throughout this research. We also gratefully acknowledge the professional English editing of Xingwang Fan in improving this article.

Funding

This work is supported by the National Natural Science Foundation of China (41801080 and 41601031), the Natural Science Foundation of Jiangsu and Jiangxi province (BK20181103 and 2018BAB213011) and the Science Foundation of Nanjing Institute of Geography and Limnology, Chinese Academy of Sciences (NIGLAS2017QD05).

References

- Acreman, M.C., Ferguson, A.J.D., 2010. Environmental flows and the European water framework directive. *Freshwater Biol.* 55, 32–48.
- Amoros-Lopez, J., Gomez-Chova, L., Alonso, L., Guanter, L., Zurita-Milla, R., Moreno, J., Camps-Valls, G., 2013. Multitemporal fusion of Landsat/TM and ENVISAT/MERIS for crop monitoring. *Int. J. Appl. Earth Obs.* 23, 132–141.
- Andreoli, R., Yesou, Y., Li, J., Desnos, Y., Shifeng, H., De Fraipont, P., 2007. Poyang Hu (Jiangxi Province, PR of China). area variations between January 2004 and June 2006 using ENVISAT low and medium resolution time series. *Geogr. Inform. Sci.* 13, 24–35.
- Ariztegui, D., Anselmetti, F.S., Robbiani, J.M., Bernasconi, S.M., Brati, E., Gilli, A., Lehmann, M.F., 2010. Natural and human-induced environmental change in southern Albania for the last 300 years – constraints from the Lake Butrint sedimentary record. *Global Planet. Change* 71, 183–192.
- Barzen, J., Engels, M., Burnham, J., Harris, J., Wu, G., 2009. Potential impacts of a water control structure on the abundance and distribution of wintering waterbirds at Poyang Lake. Unpublished report submitted to Hydro-Ecology Institute of the Yangtze Water Resources Commission. International Crane Foundation, Baraboo, Wisconsin.
- Bates, P.D., Neal, J.C., Alsdorf, D., Schumann, G.J.P., 2014. Observing global surface water flood dynamics. *Surv. Geophys.* 35, 839–852.
- Busetto, L., Meroni, M., Colombo, R., 2008. Combining medium and coarse spatial resolution satellite data to improve the estimation of sub-pixel NDVI time series. *Remote Sens. Environ.* 112, 118–131.
- Cai, X., Feng, L., Hou, X., Chen, X., 2016. Remote sensing of the water storage dynamics of large lakes and reservoirs in the Yangtze River Basin from 2000 to 2014. *Sci. Rep.-UK* 6, 36405.
- Carr, M.H., Hoctor, T.D., Goodison, C., Zwick, P.D., Green, J., Hernandez, P., McCain, C., Teisinger, J., Whitney, K., 2002. Final Report: Southeastern Ecological Framework. University of Florida, Gainesville.
- Casanova, M.T., Brock, M.A., 2000. How do depth, duration and frequency of flooding influence the establishment of wetland plant communities? *Plant Ecol.* 147, 237–250.
- Chen, B., Chen, L., Huang, B., Michishita, R., Xu, B., 2018. Dynamic monitoring of the Poyang Lake wetland by integrating Landsat and MODIS observations. *ISPRS J. Photogramm.* 139, 75–87.
- Chen, B., Huang, B., Xu, B., 2017. A hierarchical spatiotemporal adaptive fusion model using one image pair. *Int. J. Digit. Earth.* 10, 639–655.
- Chen, Y., Huang, C., Ticehurst, C., Merrin, L., Thew, P., 2013. An evaluation of MODIS daily and 8-day composite products for floodplain and wetland inundation mapping. *Wetlands* 33, 823–835.
- Dai, Z., Du, J., Li, J., Li, W., Chen, J., 2008. Runoff characteristics of the Changjiang River during 2006: effect of extreme drought and the impounding of the Three Gorges Dam. *Geophys. Res. Lett.* 35, 521–539.
- Davidson, N.C., 2014. How much wetland has the world lost? Long-term and recent trends in global wetland area. *Mar. Freshw. Res.* 65, 934–941.
- de Leeuw, J., Shankman, D., Wu, G., de Boer, W.F., Burnham, J., He, Q., Yesou, H., Xiao, J., 2010. Strategic assessment of the magnitude and impacts of sand mining in Poyang Lake, China. *Reg. Environ. Change* 10, 95–102.
- Danish Hydraulic Institute (DHI), 2007. MIKE 21 flow model: Hydrodynamic module user guide. 1–89.
- Dronova, I., Gong, P., Wang, L., 2011. Object-based analysis and change detection of major wetland cover types and their classification uncertainty during the low water period at Poyang Lake, China. *Remote Sen. Environ.* 115, 3220–3236.
- Du, Y., Xue, H.P., Wu, S.J., Ling, F., Xiao, F., Wei, X.H., 2011. Lake area changes in the middle Yangtze region of China over the 20th century. *J. Environ. Manage.* 92, 1248–1255.
- Evans, T.L., Costa, M., Telmer, K., Silva, T.S.F., 2010. Using ALOS/PALSAR and RADARSAT-2 to map land cover and seasonal inundation in the Brazilian Pantanal. *IEEE J.-STAR* 3, 560–575.
- Fang, H., Han, D., He, G., Chen, M., 2012. Flood management selections for the Yangtze River midstream after the Three Gorges Project operation. *J. Hydrol.* 432, 1–11.
- Feng, L., Hu, C., Chen, X., Zhao, X., 2013. Dramatic inundation changes of China's two largest freshwater lakes linked to the Three Gorges Dam. *Environ. Sci. Technol.* 47, 9628–9634.
- Feng, L., Hu, C.M., Chen, X.L., Tian, L.Q., Chen, L.Q., 2012. Human induced turbidity changes in Poyang Lake between 2000 and 2010: Observations from MODIS. *J. Geophys. Res.-Oceans*, 117.
- Frazier, P., Page, K., 2009. A reach-scale remote sensing technique to relate wetland inundation to river flow. *River Res. Appl.* 25, 836–849.
- Gao, F., Hilker, T., Zhu, X.L., Anderson, M.C., Masek, J.G., Wang, P.J., Yang, Y., 2015. Fusing Landsat and MODIS data for vegetation monitoring. *IEEE Geosci. Rem. Sens. M.* 3, 47–60.
- Gao, F., Masek, J., Schwaller, M., Hall, F., 2006. On the blending of the Landsat and MODIS surface reflectance: Predicting daily Landsat surface reflectance. *IEEE T.*

- Geosci. Remote 44, 2207–2218.
- Guo, H., Hu, Q., Zhang, Q., Feng, S., 2012. Effects of the three gorges dam on Yangtze river flow and river interaction with Poyang Lake, China: 2003–2008. *J. Hydrol.* 416, 19–27.
- Han, X.X., Chen, X.L., Feng, L., 2015. Four decades of winter wetland changes in Poyang Lake based on Landsat observations between 1973 and 2013. *Remote Sens. Environ.* 156, 426–437.
- Heimhuber, V., Tulbure, M.G., Broich, M., 2018. Addressing spatio-temporal resolution constraints in Landsat and MODIS-based mapping of large-scale floodplain inundation dynamics. *Remote Sens. Environ.* 211, 307–320.
- Hilker, T., Wulder, M.A., Coops, N.C., Linke, J., McDermid, G., Masek, J.G., Gao, F., White, J.C., 2009a. A new data fusion model for high spatial- and temporal-resolution mapping of forest disturbance based on Landsat and MODIS. *Remote Sens. Environ.* 113, 1613–1627.
- Hilker, T., Wulder, M.A., Coops, N.C., Seitz, N., White, J.C., Gao, F., Masek, J.G., Stenhouse, G., 2009b. Generation of dense time series synthetic Landsat data through data blending with MODIS using a spatial and temporal adaptive reflectance fusion model. *Remote Sens. Environ.* 113, 1988–1999.
- Hu, Y.X., Huang, J.L., Du, Y., Han, P.P., Huang, W., 2015. Monitoring spatial and temporal dynamics of flood regimes and their relation to wetland landscape patterns in Dongting Lake from MODIS time-series imagery. *Remote Sens.* 7, 7494–7520.
- Huang, C., Chen, Y., Wu, J.P., 2014. DEM-based modification of pixel-swapping algorithm for enhancing floodplain inundation mapping. *Int. J. Remote Sens.* 35, 365–381.
- Huang, C., Chen, Y., Zhang, S., Wu, J., 2018. Detecting, extracting and monitoring surface water from space using optical sensors – a review. *Rev. Geophys.* 1–28. <https://doi.org/10.1029/2018RG000598>.
- Hui, F.M., Xu, B., Huang, H.B., Yu, Q., Gong, P., 2008. Modeling spatial-temporal change of Poyang Lake using multitemporal Landsat imagery. *Int. J. Remote Sens.* 29, 5767–5784.
- Islam, A.S., Bala, S.K., Haque, M.A., 2010. Flood inundation map of Bangladesh using MODIS time-series images. *J. Flood Risk Manage.* 3, 210–222.
- Jenks, G.F., 1967. The data model concept in statistical mapping. *Int. Year b. Cartogr.* 7, 186–190.
- Jenks, G.F., 1977. Optimal Data Classification for Choropleth Maps. Department of Geography, University of Kansas, Occasional Paper No. 2.
- Jin, Z.Y., Xu, B., 2013. A novel compound smoother-RMMEH to reconstruct MODIS NDVI time series. *IEEE Geosci. Remote Sens. Lett.* 10, 942–946.
- Jones, K., Lanthier, Y., van der Voet, P., van Valkengoed, E., Taylor, D., Fernandez-Prieto, D., 2009. Monitoring and assessment of wetlands using Earth Observation: the GlobWetland project. *J. Environ. Manage.* 90, 2154–2169.
- Jones, S.K., Fremier, A.K., DeClerck, F.A., Smedley, D., Pieck, A.O., Mulligan, M., 2017. Big data and multiple methods for mapping small reservoirs: comparing accuracies for applications in agricultural landscapes. *Remote Sens.* 9.
- Jung, H.C., Alsdorf, D., Moritz, M., Lee, H., Vassolo, S., 2011. Analysis of the relationship between flooding area and water height in the Logone floodplain. *Phys. Chem. Earth* 36, 232–240.
- Ward, D.P., Petty, A., Setterfield, S.A., Douglas, M.M., Ferdinand, K., Hamilton, S.K., Phinn, S., 2014. Floodplain inundation and vegetation dynamics in the alligator rivers region (kakadu) of northern Australia assessed using optical and radar remote sensing. *Remote Sens. Environ.* 147, 43–55.
- Karim, F., Petheram, C., Marvanek, S., Ticehurst, C., Wallace, J., Gouweleeuw, B., 2011. The use of hydrodynamic modeling and remote sensing to estimate floodplain inundation and flood discharge in a large tropical catchment. In: Proceedings of MODSIM2011: The 19th International Congress on Modeling and Simulation, Perth, Australia, pp. 12–16.
- Khandelwal, A., Karpatne, A., Marluer, M.E., Kim, J., Lettenmaier, D.P., Kumar, V., 2017. An approach for global monitoring of surface water extent variations in reservoirs using MODIS data. *Remote Sens. Environ.* 202, 113–128.
- Klein, I., Gessner, U., Dietz, A.J., Kuenzer, C., 2017. Global WaterPack – a 250 m resolution dataset revealing the daily dynamics of global inland water bodies. *Remote Sens. Environ.* 198, 345–362.
- Kuenzer, C., Klein, I., Ullmann, T., Georgiou, E.F., Baumhauer, R., Dech, S., 2015. Remote sensing of river delta inundation: exploiting the potential of coarse spatial resolution, temporally-dense MODIS time series. *Remote Sens.* 7, 8516–8542.
- Lai, X., Shankman, D., Huber, C., Yesou, H., Huang, Q., Jiang, J., 2014a. Sand mining and increasing Poyang Lake's discharge ability: a reassessment of causes for lake decline in China. *J. Hydrol.* 519, 1698–1706.
- Lai, X.J., Jiang, J.H., Yang, G.S., Lu, X.X., 2014b. Should the Three Gorges Dam be blamed for the extremely low water levels in the middle-lower Yangtze River? *Hydrolog. Process.* 28, 150–160.
- Lan, Y., Jin, M., Yan, C., Zou, Y., 2015. Schemes of groundwater exploitation for emergency water supply and their environmental impacts on Jiujiang City, China. *Environ. Earth Sci.* 73, 2365–2376.
- Li, X., Zhang, Q., Hu, Q., Zhang, D., Ye, X., 2017. Lake flooding sensitivity to the relative timing of peak flows between upstream and downstream waterways: a case study of Poyang Lake, China. *Hydrolog. Process.* 31, 4217–4228.
- Li, Y.L., Yao, J., Zhao, G.Z., Zhang, Q., 2018. Evidences of hydraulic relationships between groundwater and lake water across the large floodplain wetland of Poyang Lake, China. *Water Sci. Tech.-W. Sup.* 18, 698–712.
- Li, Y.L., Zhang, Q., Yao, J., Werner, A.D., Li, X.H., 2014. Hydrodynamic and hydrological modeling of the Poyang Lake catchment system in China. *J. Hydrol. Eng.* 19, 607–616.
- Liao, J., Shen, G., Dong, L., 2013. Biomass estimation of wetland vegetation in Poyang Lake area using ENVISAT advanced synthetic aperture radar data. *J. Appl. Remote Sens.* 7.
- Liu, G.-H., Li, W., Zhou, J., Liu, W.-Z., Yang, D., Davy, A.J., 2006. How does the propagule bank contribute to cyclic vegetation change in a lakeshore marsh with seasonal drawdown? *Aquat. Bot.* 84, 137–143.
- Liuy, Y., Wu, G., Zhao, X., 2013. Recent declines in China's largest freshwater lake: trend or regime shift? *Environ. Res. Lett.* 8, 14010–14019.
- Lu, S.L., Jia, L., Zhang, L., Wei, Y.P., Baig, M.H.A., Zhai, Z.K., Meng, J.H., Li, X.S., Zhang, G.F., 2017. Lake water surface mapping in the Tibetan Plateau using the MODIS MOD09Q1 product. *Remote Sens. Lett.* 8, 224–233.
- Mei, X., Dai, Z., Wei, W., Gao, J., 2016. Dams induced stage-discharge relationship variations in the upper Yangtze River basin. *Hydrolog. Res.* 47, 157–170.
- Meng, J.H., Du, X., Wu, B.F., 2013. Generation of high spatial and temporal resolution NDVI and its application in crop biomass estimation. *Int. J. Digit. Earth* 6, 203–218.
- Michishita, R., Chen, L.F., Chen, J., Zhu, X.L., Xu, B., 2015. Spatiotemporal reflectance blending in a wetland environment. *Int. J. Digit. Earth* 8, 364–382.
- Michishita, R., Jin, Z.Y., Chen, J., Xu, B., 2014. Empirical comparison of noise reduction techniques for NDVI time-series based on a new measure. *ISPRS J. Photogramm.* 91, 17–28.
- Mueller, N., Lewis, A., Roberts, D., Ring, S., Melrose, R., Sixsmith, J., Lymburner, L., McIntyre, A., Tan, P., Curnow, S., Ip, A., 2016. Water observations from space: mapping surface water from 25 years of Landsat imagery across Australia. *Remote Sens. Environ.* 174, 341–352.
- Nishihiro, J., Miyawaki, S., Fujiwara, N., Washitani, I., 2004. Regeneration failure of lakeshore plants under an artificially altered water regime. *Ecol. Res.* 19, 613–623.
- Pekel, J.F., Cottam, A., Gorelick, N., Belward, A.S., 2016. High-resolution mapping of global surface water and its long-term changes. *Nature* 540, 418–422.
- Rao, Y.H., Zhu, X.L., Chen, J., Wang, J.M., 2015. An improved method for producing high spatial-resolution NDVI time series datasets with multi-temporal MODIS NDVI data and Landsat TM/ETM plus images. *Remote Sens.* 7, 7865–7891.
- Raulings, E.J., Morris, K.A.Y., Roache, M.C., Boon, P.I., 2010. The importance of water regimes operating at small spatial scales for the diversity and structure of wetland vegetation. *Freshwater Biol.* 55, 701–715.
- Rodrigues, L.N., Sano, E.E., Steenhuis, T.S., Passo, D.P., 2012. Estimation of small reservoir storage capacities with remote sensing in the Brazilian Savannah region. *Water Resour. Manage.* 26, 873–882.
- Roy, D.P., Ju, J., Lewis, P., Schaaf, C., Gao, F., Hansen, M., Lindquist, E., 2008. Multi-temporal MODIS-Landsat data fusion for relative radiometric normalization, gap filling, and prediction of Landsat data. *Remote Sens. Environ.* 112, 3112–3130.
- Scaramuzza, P., Micicjevic, E., Chander, G., 2004. SLC gap-filled products phase one methodology. *Landsat Technical Notes* 5.
- Selwood, K.E., Clarke, R.H., McGeoch, M.A., Mac Nally, R., 2017. Green tongues into the arid zone: river floodplains extend the distribution of terrestrial bird species. *Ecosystems* 20, 745–756.
- Shankman, D., Keim, B.D., Nakayama, T., Li, R., Wu, D., Remington, W.C., 2012. Hydroclimatic analysis of severe floods in China's Poyang Lake region. *Earth Interact.* 16, 1–16.
- Shankman, D., Keim, B.D., Song, J., 2006. Flood frequency in China's Poyang Lake region: trends and teleconnections. *Int. J. Climatol.* 26, 1255–1266.
- Shankman, D., Liang, Q., 2003. Landscape changes and increasing flood frequency in China's Poyang Lake Region*. *Prof. Geogr.* 55, 434–445.
- Sun, Z.D., Huang, Q., Opp, C., Hennig, T., Marold, U., 2012. Impacts and implications of major changes caused by the three gorges dam in the middle reaches of the Yangtze River, China. *Water Resour. Manage.* 26, 3367–3378.
- Tan, Z.Q., Zhang, Q., Li, M.F., Li, Y.L., Xu, X.L., Jiang, J.H., 2016. A study of the relationship between wetland vegetation communities and water regimes using a combined remote sensing and hydraulic modeling approach. *Hydrolog. Res.* 47, 278–292.
- Ticehurst, C., Dutta, D., Karim, F., Petheram, C., Guerschman, J.P., 2015. Improving the accuracy of daily modis owl flood inundation mapping using hydrodynamic modeling. *Nat. Hazards* 78, 1–18.
- Toogood, S.E., Joyce, C.B., 2009. Effects of raised water levels on wet grassland plant communities. *Appl. Veg. Sci.* 12, 283–294.
- Tulbure, M.G., Broich, M., Stehman, S.V., Kommareddy, A., 2016. Surface water extent dynamics from three decades of seasonally continuous Landsat time series at sub-continental scale in a semi-arid region. *Remote Sens. Environ.* 178, 142–157.
- Turvey, S.T., Barrett, L.A., Hart, T., Collen, B., Yujiang, H., Lei, Z., Xinqiao, Z., Xianyan, W., Yadong, H., Kaiya, Z., 2010. Spatial and temporal extinction dynamics in a freshwater cetacean. *Proc. Roy. Soc. Lond. B: Biol. Sci.* 277, 3139–3147.
- Wang, P., Lai, G.Y., Li, L., 2015. Predicting the hydrological impacts of the Poyang Lake project using an EFDC model. *J. Hydrol. Eng.* 20.
- Weng, Q.H., Fu, P., Gao, F., 2014. Generating daily land surface temperature at Landsat resolution by fusing Landsat and MODIS data. *Remote Sens. Environ.* 145, 55–67.
- Williamson, C.E., Saros, J.E., Vincent, W.F., Smol, J.P., 2009. Lakes and reservoirs as sentinels, integrators, and regulators of climate change. *Limnol. Oceanogr.* 54, 2273–2282.
- Winemiller, K.O., McIntyre, P.B., Castello, L., Fluet-Chouinard, E., Giarrizzo, T., Nam, S., Baird, I.G., Darwall, W., Lujan, N.K., Harrison, I., Stiassny, M.L.J., Silvano, R.A.M., Fitzgerald, D.B., Peilicce, F.M., Agostinho, A.A., Gomes, L.C., Albert, J.S., Baran, E., Petrere, M., Zarfl, C., Mulligan, M., Sullivan, J.P., Arantes, C.C., Sousa, L.M., Koning, A.A., Hoeinghaus, D.J., Sabaj, M., Lundberg, J.G., Armbruster, J., Thieme, M.L., Petry, P., Zuanon, J., Vilara, G.T., Snoeks, J., Ou, C., Rainboth, W., Pavanelli, C.S., Akama, A., van Soesbergen, A., Saenz, L., 2016. Balancing hydropower and biodiversity in the Amazon, Congo, and Mekong. *Science* 351, 128–129.
- Wu, G.P., Liu, Y.B., 2015. Capturing variations in inundation with satellite remote sensing in a morphologically complex, large lake. *J. Hydrol.* 523, 14–23.
- Wu, M.Q., Huang, W.J., Niu, Z., Wang, C.Y., Li, W., Yu, B., 2018. Validation of synthetic daily Landsat NDVI time series data generated by the improved spatial and temporal

- data fusion approach. *Inform. Fusion.* 40, 34–44.
- Wu, M.Q., Niu, Z., Wang, C.Y., Wu, C.Y., Wang, L., 2012. Use of MODIS and Landsat time series data to generate high-resolution temporal synthetic Landsat data using a spatial and temporal reflectance fusion model. *J. Appl. Remote Sens.* 6.
- Wu, M.Q., Wu, C.Y., Huang, W.J., Niu, Z., Wang, C.Y., Li, W., Hao, P.Y., 2016. An improved high spatial and temporal data fusion approach for combining Landsat and MODIS data to generate daily synthetic Landsat imagery. *Inform. Fusion.* 31, 14–25.
- Xu, Y., Lai, X., Zhou, C., 2010. Water surface change detection and analysis of bottomland submersion-emersion of wetlands in Poyang Lake Reserve using ENVISAT ASAR data. *China Environ. Sci.* 30, 57–63 (In Chinese).
- Yamazaki, D., Trigg, M.A., Ikeshima, D., 2015. Development of a global similar to 90 m water body map using multi-temporal Landsat images. *Remote Sen. Environ.* 171, 337–351.
- Yao, J., Zhang, Q., Ye, X.C., Zhang, D., Bai, P., 2018. Quantifying the impact of bathymetric changes on the hydrological regimes in a large floodplain lake: Poyang Lake. *J. Hydrol.* 561, 711–723.
- Zhang, L., Lu, J., Chen, X., Liang, D., Fu, X., Sauvage, S., Sanchez Perez, J.-M., 2017a. Stream flow simulation and verification in ungauged zones by coupling hydrological and hydrodynamic models: a case study of the Poyang Lake ungauged zone. *Hydrolog. Earth Syst. Sci.* 21, 5847–5861.
- Zhang, L.L., Yin, J.X., Jiang, Y.Z., Wang, H., 2012. Relationship between the hydrological conditions and the distribution of vegetation communities within the Poyang Lake National Nature Reserve, China. *Ecol. Inform.* 11, 65–75.
- Zhang, P., Chen, X., Lu, J., Zhang, W., 2015. Assimilation of remote sensing observations into a sediment transport model of China's largest freshwater lake: spatial and temporal effects. *Environ. Sci. Pollut. R.* 22, 18779–18792.
- Zhang, Q., Ye, X.C., Werner, A.D., Li, Y.L., Yao, J., Li, X.H., Xu, C.Y., 2014. An investigation of enhanced recessions in Poyang Lake: comparison of Yangtze River and local catchment impacts. *J. Hydrol.* 517, 425–434.
- Zhang, X.L., Zhang, Q., Werner, A.D., Tan, Z.Q., 2017b. Characteristics and causal factors of hysteresis in the hydrodynamics of a large floodplain system: Poyang Lake (China). *J. Hydrol.* 553, 574–583.
- Zhang, Y.L., Jeppesen, E., Liu, X.H., Qin, B.Q., Shi, K., Zhou, Y.Q., Thomaz, S.M., Deng, J.M., 2017c. Global loss of aquatic vegetation in lakes. *Earth-Sci. Rev.* 173, 259–265.
- Zhao, P., Tang, X., Tang, J., Wang, C., 2013. Assessing water quality of Three Gorges Reservoir, China, over a five-year period from 2006 to 2011. *Water Resour. Manage.* 27, 4545–4558.
- Zhao, X., Stein, A., Chen, X.-L., 2011. Monitoring the dynamics of wetland inundation by random sets on multi-temporal images. *Remote Sen. Environ.* 115, 2390–2401.
- Zhao, Y.Q., Huang, B., Song, H.H., 2018. A robust adaptive spatial and temporal image fusion model for complex land surface changes. *Remote Sen. Environ.* 208, 42–62.
- Zhu, X.L., Chen, J., Gao, F., Chen, X.H., Masek, J.G., 2010. An enhanced spatial and temporal adaptive reflectance fusion model for complex heterogeneous regions. *Remote Sen. Environ.* 114, 2610–2623.